RESEARCH ARTICLE





Energetics and structure of SiC(N)(O) polymer-derived ceramics

Gerson J. Leonel^{1,2} | Xin Guo³ | Gurpreet Singh⁴ | Christel Gervais⁵ | Alexandra Navrotsky^{1,2} 🕞

¹School of Molecular Sciences and Center for Materials of the Universe, Arizona State University, Tempe, Arizona, USA ²Navrotsky Eyring Center for Materials of

the Universe, School of Molecular Sciences, Arizona State University, Tempe, Arizona, USA

³Eyring Materials Center, Arizona State University, Tempe, Arizona, USA

⁴Mechanical and Nuclear Engineering Department, Kansas State University, Manhattan, Kansas, USA

⁵Sorbonne Université, CNRS UMR 7574, Collège de France, LCMCP, Paris, France

Correspondence

Alexandra Navrotsky, School of Molecular Sciences and Center for Materials of the Universe, Arizona State University. Tempe, AZ 85287, USA.

Email: Alexandra.navrotsky@asu.edu

Funding information

National Science Foundation (NSF) Partnerships for International Research and Education (PIRE), Grant/Award Number: #1743701

Abstract

This study presents new experimental data on the thermodynamic stability of SiC(O) and SCN(O) ceramics derived from the pyrolysis of polymeric precursors: SMP-10 (polycarbosilane), PSZ-20 (polysilazane), and Durazane-1800 (polysilazane) at 1200°C. There are close similarities in the structure of the polysilazanes, but they differ in crosslinking temperature. High-resolution X-ray photoelectron spectroscopy shows notable differences in the microstructure of all polymer-derived ceramics (PDCs). The enthalpies of formation ($\Delta H^{\circ}_{f, elem}$) of SiC(O) (from SMP-10), SCN(O) (from PSZ-20), and SCN(O) (from Durazane-1800) are -20 ± 4.63 , -78.55 ± 2.32 , and -85.09 ± 2.18 kJ/mol, respectively. The PDC derived from Durazane-1800 displays greatest thermodynamic stability. The results point to increased thermodynamic stabilization with addition of nitrogen to the microstructure of PDCs. Thermodynamic analysis suggests increased thermodynamic drive for forming SiCN(O) microstructures with an increase in the relative amount of SiN_xC_{4-x} mixed bonds and a decrease in silica. Overall, enthalpies of formation suggest superior stabilizing effect of SiN_xC_{4-x} compared to SiO_xC_{4-x} mixed bonds. The results indicate systematic stabilization of SiCN(O) structures with decrease in silicon and oxygen content. The destabilization of PDCs resulting from higher silicon content may reach a plateau at higher concentrations.

KEYWORDS

glass-ceramics, polymer precursor, silicon carbonitride, silicon oxycarbide, thermodynamics

1 INTRODUCTION

Recent technological advances continue to fuel research and development of materials for application under extreme conditions.¹⁻³ Typically, materials like polymerderived SiOCs, and SiCNs with high chemical, thermal, and mechanical stability are desired, as they may possess properties comparable to refractory ceramics such as ZrB₂ for which single-source precursors are not commercially available. 4-9 This has led to increase in the popularity of ceramics in various industries, including their application as sensors, mechanical seals, and ceramic bearing. 10-12 By convention, ceramic systems are produced by high temperature sintering of powder mixtures. 13-15 Such techniques may not permit swift tunability of the microstructure and dimensions of the ceramics, thus deeming the synthesis process inefficient. 16-19 Other common approaches for synthesis of binary SiC and ternary SiOC systems include chemical vapor deposition and spark plasma sintering. The former is typically preferred for the production of

thin films in the semiconductor industry.^{20–24} Recently, polymer-derived ceramics (PDCs) became a popular synthesis route to overcome conventional limitations.

PDCs belong to a class of ceramics derived from the crosslinking followed by high temperature pyrolysis of polymeric precursors. 25-28 This route permits fine tuning of the microstructure in PDCs by controlling side groups in the backbone of the polymer precursor. 12,29,30 The low viscosity of preceramic polymers permits their use as precursors for polymer infiltration and pyrolysis (PIP) in the development of ceramic matrix composites (CMCs).31-34 Recent studies demonstrated tunability in the dimensions of PDCs through utilization of molding techniques.³⁵ This permits development of polymeric shapes that can be patterned by photolithography, plasma etching, and laser ablation techniques. These shapes can then be pyrolyzed into ceramics.^{36,37} The viscosity of the polymer can be adjusted for extrusion-based 3D printing, and this permits more controlled tunability of the dimensions of PDCs during processing.³⁸⁻⁴⁰ The ease in tunability of microstructure and dimensions of the ceramics makes the PDC route attractive for large scale application.

Typically, the microstructure of PDCs consists of regions containing X-ray amorphous free carbon and domains of the SiO_xC_{4-x} or SiN_xC_{4-x} mixed bonding network, where $0 \le x \le 4.41,42$ This complexity makes assessment of structure-property relation challenging. 43-45 Nonetheless, spectroscopic techniques like Fourier transform infrared spectroscopy (FTIR), X-ray photoemission spectroscopy (XPS), and nuclear magnetic resonance (NMR) can be used to determine bonding speciation in the structure of PDCs.46,47

Recently, PDCs fueled the development of commercial and industrial polymeric precursors for the synthesis of high temperature ceramics with tunable compositions. 48-51 Typically, SiC PDCs are less thermally stable than SiCN and SiOCs ceramics, which results in early crystallization of amorphous domains in binary SiC ceramics.⁵² Most PDC studies emphasize the application of PDCs,^{53,54} only few investigate the free-energy landscape of ceramic materials derived through the polymeric route. As ceramics derived from industrial precursors increase in popularity, it is essential to understand their structure-property relation, especially the influence of chemistry and structure on the thermodynamic stability of PDCs. Such systematic studies help in the development of a framework for the predictive design and synthesis of PDCs with high thermodynamic stability and desired functionality.

This work investigates three ceramic samples derived from preceramic polymers: SMP-10, PSZ-20, and Durazane-1800. We report the synthesis, characterization,

and thermochemical analysis of the PDCs synthesized at 1200°C, in flowing argon atmosphere. Systematic variations in the composition of the samples lead to differences in enthalpies of formation. This permits quantitative assessment of the interconnectivity between the chemistry, structure, bonding, and thermodynamic stability in PDCs. Chemical and structural characterization of the specimen are performed by XPS, high-resolution XPS (HR-XPS), Raman spectroscopy, FTIR, and NMR. High temperature oxide melt solution calorimetry is employed to assess thermodynamic stability of the materials. The new compositions explored in this work fill-in gaps of composition-stability relations in PDCs.

EXPERIMENTAL METHODS

2.1 **Materials**

The ceramics are derived from polymeric precursors: SMP-10 (SiC precursor, from Starfire Systems), PSZ-20 (SiCN precursor, from KiON Ceraset), and Durazane-1800 (SiCN precursor, from Merck). SMP-10 only contains Si-C-H bonds, whereas Durazane-1800 and PSZ-20 contain additional Si-N bonds. The SiCN precursors have comparable structures, the only difference could be in the ratio of Si-vinyl to Si-CH₃ groups. Structure of the oligomers is shown in Figure 1. We do not use crosslinking catalysts during synthesis of the PDCs.

2.2 Crosslinking

The single-source precursors (without the addition of catalyst) are employed for synthesis of the SiC and SiCNs. The as-received precursors are stored in a laboratory refrigerator, the specimens are left to equilibrate at room temperature before crosslinking. Crosslinking is performed in a beaker using a Benchmark hot plate ($T_{\text{max}} \sim 300^{\circ}\text{C}$) under magnetic stirring. SMP-10 (polycarbosilane) and PSZ-20 (polysilazane) oligomers are crosslinked into infusible solids at ~250°C, using ~5°C/min ramping rate, and 4 h hold at the final crosslinking temperature, in a glove box employing nitrogen atmosphere (~0.1 ppm oxygen). Durazane-1800 (polysilazane) has a higher curing temperature (~300°C). The cross-linked polymers are then processed for pyrolysis. This procedure is decided based on curing requirements (time, atmosphere, and raping rate) of the precursors, comparable to experimental parameters used in previous works.51,55,56

.5512916, 2023, 8, Downloaded from https://ceramics

.com/doi/10.1111/jace.19153 by Kansas State University, Wiley Online Library on [18/10/2023]. See the Terms and Conditions

FIGURE 1 Structure of oligomers used for synthesis of the ceramic powders at 1200°C, under flowing argon atmosphere.

2.3 | Pyrolysis

A Netzsch STA 409 differential scanning calorimeter cell, using alumina crucibles is employed for pyrolysis of the cross-linked precursors. The instrument permits precise temperature control and a low temperature gradient in samples. The specimens are pyrolyzed under flowing argon (~50 mL/min). The samples are heated from room temperature to 1200°C at a ramping rate of 2°C/min. During heating, the samples are held at 400°C for 1 h, this ensures complete crosslinking of the precursor, as the hot plate used for crosslinking can only achieve $T_{\rm max} \sim 300$ °C. The ceramics formed during high temperature pyrolysis are then ground into fine powders.

2.4 | Characterization

XPS experiments are performed by use of a Kratos AXIS Supra+ with a monochromatic Al K_{α} + ion beam (beam energy = 1486.6 eV). Raman spectroscopy experiments employed a custom-built multi-wavelengths system with a 532 nm green laser at a power of 74 mW with a 50× microscope objective. X-ray diffraction (XRD) experiments are performed at ambient conditions by use of a benchtop Bruker D2 powder diffractometer (nickel-filtered CuK_{α} radiation, wavelength = 1.5418 Å). FTIR experiments are performed by employing a benchtop Bruker TENSOR with platinum ATR accessory. Thermal analyses are performed in an LABSYS evo DTA/DSC, under flowing argon atmosphere. Solid-state ²⁹Si MAS NMR spectra were recorded on a Bruker AVANCE 300 spectrometer ($B_0 = 7.0$ T, $v_0(^1\text{H}) = 300.29 \text{ MHz}, \text{ and } v_0(^{29}\text{Si}) = 59.66 \text{ MHz}) \text{ using}$ a 4 mm Bruker probe and spinning frequency of 12 kHz. Single-pulse ²⁹Si NMR MAS spectra were recorded with recycle delays of 60 s. Chemical shift values were referenced to tetramethylsilane. The spectra were simulated with the DMFIT program.⁵⁷

2.5 | Calorimetry

Enthalpies of formation from elements $(\Delta H^{\circ}_{\text{f,elem}})$ and components ($\Delta H^{\circ}_{f, \text{comp}}$) are obtained by use of thermochemical cycles and enthalpies of dissolution (ΔH°_{dis}) obtained by high temperature oxide melt solution calorimetry at 800°C. The calorimetric experiments are conducted by use of a commercial twin Calvet type Setaram Alexsys calorimeter, employing molten sodium molybdate (3Na₂O·4MoO₃) as solvent. An amount of ~5 mg of sample is weighed using a Mettler Toledo microbalance with 10 μ g accuracy. The weighed sample is pressed into a pellet using a 1.5 mm tungsten die. The palletized sample is then dropped from room temperature into the melt in the hot calorimeter for oxidative dissolution. To maintain an oxidative environment, the melt is continuously under oxygen bubbling (40 mL/min). Oxygen flushing (100 mL/min) above the melt is used to expel any gases evolved during dissolution; ensuring a constant environment in the reaction chamber. This is a well-established technique, and more details are provided in previous studies. 58,59 During dissolution of SiC(O) and SiCN(O) samples, N, and C evolve as N2, and CO2, respectively, and Si is oxidized and precipitates as high temperature cristobalite (SiO₂).⁴⁶

The dissolution of SiCN(O) is described as follows:

$$Si_aO_bC_cN_d$$
 (s, 25°C) + ((2 (a + c) – b) /2) O_2 (g, 800°C)
 $\rightarrow aSiO_2$ (s, 800°C) + cCO_2 (g, 800°C) + $d/2N_2$
(g, 800°C) $\Delta H^{\circ}_{dis,SiCN(O)}$ (1)

Reaction (2) describes dissolution of SiOC in the melt:

Si_aO_bC_c (s, 25°C) + ((2 (a + c) − b) /2) O₂ (g, 800°C)
→ aSiO₂ (s, 800°C) + cCO₂ (g, 800°C)
$$\Delta H^{\circ}_{\text{dis,SiC(O)}}$$

(2)

litions) on Wiley Online Library for rules of use; OA articles are governed by the applicable Creative Commons License

iournal

Thermochemical cycle for calculation of enthalpy of formation of SiCN(O) from elements $\Delta H^{\circ}_{f, elem}$.

Enthalpies of formation from the elements $(\Delta H^{\circ}_{\mathrm{f, elem}})$ $a \operatorname{Si}(\mathrm{s}, 25^{\circ}\mathrm{C}) + c \operatorname{C}(\mathrm{s}, 25^{\circ}\mathrm{C}) + b/2 \operatorname{O}_{2}(\mathrm{g}, 25^{\circ}\mathrm{C}) + d/2 \operatorname{N}_{2}(\mathrm{g}, 25^{\circ}\mathrm{C}) \rightarrow \operatorname{Si}_{a} \operatorname{O}_{b} \operatorname{C}_{c} \operatorname{N}_{d}(\mathrm{s}, 25^{\circ}\mathrm{C})$	(s, 25°C)
$\Delta H^{\circ}_{\mathrm{f, elem}} = ?$	ΔH (kJ/mol)
$\mathbf{Si}_a \mathbf{O}_b \mathbf{C}_c \mathbf{N}_d$ (s, 25°C) + ((2(a + c) - b)/2) \mathbf{O}_2 (g, 800°C) \rightarrow a \mathbf{SiO}_2 (s, 800°C) + c \mathbf{CO}_2 (g, 800°C) 800°C)	C) + $d/2 N_2$ (g, $\Delta H^{\circ}_{dis, SiCN(O)}$
$Si(s, 25^{\circ}C) + O_2(g, 800^{\circ}C) \rightarrow SiO_2(s, 800^{\circ}C)$	$\Delta H_2 = -883.13 \pm 2.1$
$C(s, 25^{\circ}C) + O_2(g, 800^{\circ}C) \rightarrow CO_2(g, 800^{\circ}C)$	$\Delta H_3 = -381.35 \pm 0.13$
$O_2(g, 25^{\circ}C) \to O_2(g, 800^{\circ}C)$	$\Delta H_4 = 25.34 \pm 0.10$
$N_2(g, 25^{\circ}C) \to N_2(g, 800^{\circ}C)$	$\Delta H_5 = 24.77 \pm 0.10$
$\Delta \mathbf{H}^{\circ}_{f, \text{ elem}} = -\Delta \mathbf{H}^{\circ}_{\text{dis, SiCN}} + a\Delta H_2 + c\Delta H_3 + (b/2)\Delta H_4 + (d/2)\Delta H_5$	$\Delta oldsymbol{H}^{\circ}_{ ext{ f, elem}}$

Enthalpy of formation of SiC(O) and SiCN(O) from elements is described by reactions (3) and (4), respectively:

$$a\text{Si}(s, 25^{\circ}\text{C}) + b/2\text{O}_{2}(g, 25^{\circ}\text{C}) + c\text{C}(s, 25^{\circ}\text{C})$$

$$\rightarrow \text{Si}_{a}\text{O}_{b}\text{C}_{c}(s, 25^{\circ}\text{C}) \quad \Delta H^{\circ}_{f,\text{elem}} =? \qquad (3)$$

$$a\text{Si}(s, 25^{\circ}\text{C}) + c\text{C}(s, 25^{\circ}\text{C}) + b/2\text{O}_{2}(g, 25^{\circ}\text{C}) + d/2\text{N}_{2}$$

$$(g, 25^{\circ}\text{C}) \rightarrow \text{Si}_{a}\text{O}_{b}\text{C}_{c}\text{N}_{d}(s, 25^{\circ}\text{C})(s, 25^{\circ}\text{C}) \quad \Delta H^{\circ}_{f,\text{elem}} =?$$

$$(4)$$

Reactions (5) and (6) describe formation of SiC(O) and SiCN(O) relative to crystalline components (β -SiC, SiO₂ [cristobalite], β -Si₃N₄, and C [graphite]):

$$(a - (b/2)) \operatorname{SiC}(s, 25^{\circ}C) + (b/2) \operatorname{SiO}_{2}(s, 25^{\circ}C)$$

$$+ (c - (a - (b/2))) \operatorname{C}(s, 25^{\circ}C) \rightarrow \operatorname{Si}_{a} \operatorname{O}_{b} \operatorname{C}_{c}$$

$$(s, 25^{\circ}C) \Delta H^{\circ}_{f,comp} = ?$$

$$(a - (b/2) - (3d/4)) \operatorname{SiC}(s, 25^{\circ}C) + (b/2) \operatorname{SiO}_{2}(s, 25^{\circ}C)$$

$$+ (d/4) \operatorname{Si}_{3} \operatorname{N}_{4}(s, 25^{\circ}C) + (c - (a - (b/2) - (3d/4)))$$

$$\operatorname{C}(s, 25^{\circ}C) \rightarrow \operatorname{Si}_{a} \operatorname{O}_{b} \operatorname{C}_{c} \operatorname{N}_{d}(s, 25^{\circ}C) (s, 25^{\circ}C) \Delta H^{\circ}_{f,comp} = ?$$

$$(6)$$

By identifying the initial and final state of the system during dissolution, we employ thermodynamic cycles (Tables 1-4) for thermochemical calculation of enthalpies of formation.

3 **RESULTS AND DISCUSSION**

FTIR experiments permit identification of functional groups in the structure of cross-linked polymeric precursors and corresponding ceramics. The results in Figure 2a confirm presence of organic groups in the structure of cross-linked precursors. The functional groups in the spec-

tra are consistent with structure of the oligomers. The intensity of peaks in the spectra is proportional to the relative amounts of the corresponding bonds. The cross-linked polysilazanes (PSZ-20 and Durazane-1800) have comparable structures, and the higher intensity of Si-CH2-Si stretching vibrational peaks (1020 cm⁻¹) in Durazane-1800 may indicate higher relative amounts of Si-CH₂ bonds per unit volume. 60,61 Figure 2b summarizes results from FTIR of the PDCs pyrolyzed at 1200°C. The spectra in Figure 2b suggest absence of C-H, N-H, and Si-H bonds, which is consistent with evolution of H as organics during high temperature pyrolysis. The results in Figure 2b further point to the presence of C=C (~1600 cm⁻¹) and maybe some Si-O-Si (\sim 1060 cm⁻¹) bonds in the samples. ^{62,63} Additionally, Si-N bonds are identified in PDCs derived from Durazane-1800 and PSZ-20. PDCs derived from SMP-10 yield SiC ceramics, whereas each PSZ-20 and Durazane-1800 are precursors for SiCN. It is well known that it is difficult to obtain oxygen-free SiCNs and SiCs, especially since it is in part an impurity in the precursors. ^{64,65} The peaks assigned to Si-O bonds in the structure of the polymeric precursors and corresponding PDCs may indicate oxygen contamination during processing; therefore, to acknowledge the presence of oxygen, we refer to the pyrolyzed materials as SiC(O) and SiCN(O) ceramics.

Thermogravimetric (TG) and differential scanning calorimetric (DSC) curves during pyrolysis are shown in Figure 3. To account for buoyancy effect of the carrier gas, baseline TG-DSC signal (empty crucible) was subtracted from the sample run. All precursors undergo ~76 wt% loss between ambient temperature and 1200°C. Overall, the cross-linked precursors display acceptable ceramic yields of about 76%, even without the use of crosslinking catalysts, and this is in good agreement with previous work.⁵⁶ The exothermic peaks near 200°C likely correspond to further crosslinking of precursors.⁶⁶ In these samples, the initiation of polymer to ceramic conversion may be indicated by the exothermic DSC peak near 400°C.67 Durazane-1800 displays the highest crosslinking

5512916, 2023, 8, Downloaded from https://ceramics.onlinelibrary.wiley.com/doi/10.1111/jace.19153 by Kansas State University, Wiley Online Library on [18/10/2023]. See the Terms and Conditions

nditions) on Wiley Online Library for rules of use; OA articles are governed by the applicable Creative Commons License

Thermochemical cycle for calculation of enthalpy of formation of SiCN(O) from components $\Delta H^{\circ}_{i, comp}$. FABLE 2

Enumarples of infinite form components (AA $_{\rm f, comp}$) $(a - (b/2) - (3d/4))$ SiC (s, 25°C) $+ (b/2)$ SiO ₂ (s, 25°C) $+ (d/4)$ Si ₃ N ₄ (s, 25°C) $+ (c - (a - (b/2) - (3d/4)))$ C (s, 25°C) \rightarrow Si _a O _b C _c N _d (s, 25°C) (s, 25°C) \rightarrow	∆H (kJ/mol)
$\mathbf{Si_aO_bC_cN_d}$ (s, 25°C) + $((2(a+c)-b)/2)$ O ₂ (g, 800°C) $\rightarrow a$ SiO ₂ (s, 800°C) + c CO ₂ (g, 800°C) + $d/2$ N ₂ (g, 800°C)	$\Delta H^{\circ}_{ m dis,SiCN(0)}$
$SiO_2(s, 25^{\circ}C) \rightarrow SiO_2(s, 800^{\circ}C)$	$\Delta H_2 = 50.1 \pm 0.10$
$SiC(s, 25^{\circ}C) + 2O_2(g, 800^{\circ}C) \rightarrow SiO_2(s, 800^{\circ}C) + CO_2(g, 800^{\circ}C)$	$\Delta H_3 = -1192.28 \pm 2.15$
Si_3N_4 (s, $25^{\circ}C$) + $3O_2$ (g, $800^{\circ}C$) $\rightarrow 3SiO_2$ (s, $800^{\circ}C$) + $2N_2$ (g, $800^{\circ}C$)	$\Delta H_4 = -1770.95 \pm 4.0$
$C(s, 25^{\circ}C) + O_2(g, 800^{\circ}C) \rightarrow CO_2(g, 800^{\circ}C)$	$\Delta H_5 = -381.35 \pm 0.13$
$\Delta H_{\text{f,comp}} = -\Delta H_{\text{dis, SICN(0)}} + (b/2)\Delta H_2 + (a - (b/2) - (3d/4))\Delta H_3 + (d/4)\Delta H_4 + (c - (a - (b/2) - (3d/4)))\Delta H_5$	ΔH° f, comp

temperature (~300°C) and lowest ceramic yield relative to the cross-linked precursor (~75.8 wt%). In contrast, PSZ-20 cross-linked polymers display lower thermal stability with an onset decomposition temperature of ~250°C. Figure 3 further shows that SMP-10 (polycarbosilane) has the greatest ceramic yield and lowest crosslinking temperature (~200°C). The crosslinking temperatures suggested from DSC curves (Figure 3) are consistent with initial crosslinking temperatures of the oligomers, which point to PSZ-20 as a lower temperature curing polysilazane. These results show significant differences in the thermal behavior of cross-linked polymers, even in polysilazanes (PSZ-20 and Durazane-1800) with comparable chemical structures (see Figures 1 and 2). Overall, major changes in mass conclude near 900°C, however, SMP-10 undergoes minor secondary exothermic mass loss between 900 and 1150°C, which may indicate carbothermal reduction of silica networks (SiO₂) by free carbon and this results in the crystallization of SiC domains. 68,69

XRD permits identification of crystallization and can help determine structural differences in crystalline materials including some SiC PDC fibers. 46 Typically, PDCs pyrolyzed at lower temperatures are amorphous. 30,70 At high temperatures, crystallization in PDCs is promoted by carbothermal reduction.^{71–73} The XRD patterns of the PDCs are summarized in Figure 4 and the results point to growth of poorly crystalline β -SiC grains in the SiC(O) derived from SMP-10. This may indicate carbothermal reduction, which results in phase separation and crystallization of amorphous domains. 71,74,75 The XRD patterns suggest amorphous microstructures in SiCN(O) samples derived from PSZ-20 and Durazane-1800. The results summarized in Figure 4 suggest superior resistance to crystallization in SiCN(O)s than in SiC(O)s PDCs, which is expected, as addition of N to SiC structures has been found to result in higher persistence to thermal degradation and crystallization.⁵² Differences in the crystallization temperature/rates of these materials likely result from kinetic rather than thermodynamic factors, since in general PDCs evolve toward thermodynamically more stable structures with increasing pyrolysis temperature 30,58,76-78 Some kinetic factors for consideration may include difference in the activation energy for carbothermal reduction of distinct oxides and nitrides domains, as well as dissimilarities in the diffusion rate of different species.30,76

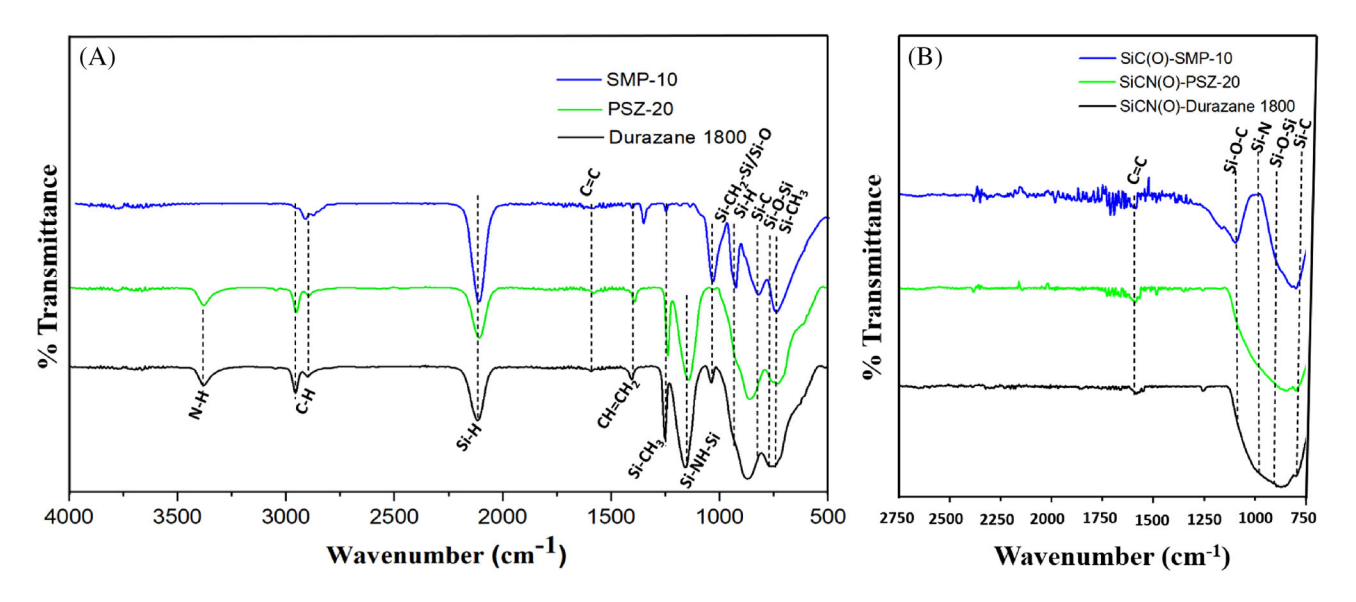
The types of carbon in the microstructure of the ceramic powders can be identified by Raman spectroscopy. The spectra are collected between 900 and 1900 Raman shift (cm⁻¹) and the results are summarized in Figure 5. D (~1330 cm⁻¹) and G (~1600 cm⁻¹) bands correspond to presence of sp²-hybridized disordered and graphitic-like carbons, respectively.^{36,46} The integrated intensity of D

Thermochemical cycle for calculation of enthalpy of formation of SiC(O) from elements $\Delta H^{\circ}_{f, elem}$

Enthalpies of formation from the elements $(\Delta H^{\circ}_{f, \text{ elem}})$ $a \operatorname{Si}(s, 25^{\circ} \text{C}) + b/2 \operatorname{O}_{2}(g, 25^{\circ} \text{C}) + c \operatorname{C}(s, 25^{\circ} \text{C}) \rightarrow \operatorname{Si}_{a} \operatorname{O}_{b} \operatorname{C}_{c}(s, 25^{\circ} \text{C}) \Delta H^{\circ}_{f, \text{ elem}} = ?$	ΔH (kJ/mol)
$Si_aO_bC_c$ (s, 25°C) + (((2a) + (2c) – b))/2) O_2 (g, 800°C) $\rightarrow a$ SiO_2 (s, 800°C) + c CO_2 (g, 800°C)	$\Delta H^{\circ}_{ m \ dis, \ SiOC}$
$Si(s, 25^{\circ}C) + O_2(g, 800^{\circ}C) \rightarrow SiO_2(s, 800^{\circ}C)$	$\Delta H_2 = -883.13 \pm 2.1$
$C(s, 25^{\circ}C) + O_2(g, 800^{\circ}C) \rightarrow CO_2(g, 800^{\circ}C)$	$\Delta H_3 = -381.35 \pm 0.13$
$O_2(g, 25^{\circ}C) \to O_2(g, 800^{\circ}C)$	$\Delta H_4 = 25.34 \pm 0.10$
$\Delta H^{\circ}_{f, \text{ elem}} = -\Delta H^{\circ}_{\text{dis, SiOC}} + a \Delta H_2 + c \Delta H_3 + (b/2) \Delta H_4$	$\Delta H^{\circ}_{ m f,elem}$

Thermochemical cycle for calculation of enthalpy of formation of SiC(O) from components $\Delta H^{\circ}_{f, \text{comp}}$.

Enthalpies of formation from components $(\Delta H^{\circ}_{f, \text{comp}})$ $(a - (b/2)) \text{ SiC}(s, 25^{\circ}\text{C}) + (b/2) \text{ SiO}_{2}(s, 25^{\circ}\text{C}) + (c - (a - (b/2))) \text{ C}(s, 25^{\circ}\text{C}) \rightarrow \text{Si}_{a}\text{O}_{b}\text{C}_{c}(s, 25^{\circ}\text{C})$	
$\Delta H^{\circ}_{f, \text{ comp}} = ?$	$\Delta H (kJ/mol)$
$Si_aO_bC_c$ (s, 25°C) + (((2a) + (2c) – b)/2) O_2 (g, 800°C) $\rightarrow a$ SiO_2 (s, 800°C) + c CO_2 (g, 800°C)	$\Delta H^{\circ}_{ m dis,SiOC}$
$SiO_2(S, 25^{\circ}C) \rightarrow SiO_2(s, 800^{\circ}C)$	$\Delta H_2 = 50.1 \pm 0.10$
$SiC(S, 25^{\circ}C) + 2O_2(g, 800^{\circ}C) \rightarrow SiO_2(s, 800^{\circ}C) + CO_2(g, 800^{\circ}C)$	$\Delta H_3 = -1192.28 \pm 2.15$
$C(S, 25^{\circ}C) + O_2(g, 800^{\circ}C) \rightarrow CO_2(g, 800^{\circ}C)$	$\Delta H_4 = -381.35 \pm 0.13$
$\Delta H^{\circ}_{f, \text{ comp}} = -\Delta H^{\circ}_{\text{dis, SiOC}} + (b/2) \Delta H_2 + (a - (b/2)) \Delta H_3 + (c - (a - (b/2))) \Delta H_4$	$\Delta H^{\circ}_{ m f,comp}$



Fourier transform infrared spectroscopy (FTIR) spectra of (A) cross-linked polymeric precursors, SMP-10, PSZ-20, and Durazane-1800 (B) polymer-derived ceramics (PDCs) derived from preceramic polymers at 1200°C, in flowing argon.

 $(I_{\rm D})$ and G $(I_{\rm G})$ bands at full width at half maximum permit assessment of the D $(I_D)/G$ (I_G) ratio of bonding speciation.⁵⁸ It appears that all samples contain greater amounts of disordered (relative to graphitic) carbons. D" (1490-1504 cm⁻¹) and T (1204-1232 cm⁻¹) bands, which are obtained from curve fitting, indicate presence of significant amounts of amorphous carbon and sp²-sp³ bonds, respectively, in the microstructure of all specimens. For the SiCN(O)s, the sample derived from Durazane-1800 displays largest integrated intensities of D" and T (relative to G and D) bands. 36,79,80 This points to lower relative amount of amorphous free carbon and sp²-sp³ bonds in SiCN(O) derived from PSZ-20.

XPS is efficient for identification of different Si 2p, C 1s, O 1s, and N 1s bonds; however, it is challenging to identify different SiN_xC_{4-x} bonds by XPS alone. NMR is powerful for characterization of short range order in ceramics, and analysis of the spectra permits differentiation of SiN_xC_{4-x} mixed bonding environments in PDCs. 58,70,79 Typically, ²⁹Si MAS NMR peak shifts are associated with different coordination environments (oxygen in SiO_xC_{4-x} or nitrogen in SiN_xC_{4-x} mixed bonds).⁸¹ ²⁹Si MAS NMR

1512916, 2023, 8, Downloaded from https://ecramics.onlinelibrary.wiley.com/doi/10.1111/jace.19153 by Kansas State University, Wiley Online Library on [18/10/2023]. See the Terms

ditions) on Wiley Online Library for rules of use; OA articles are governed by the applicable Creative Commons License

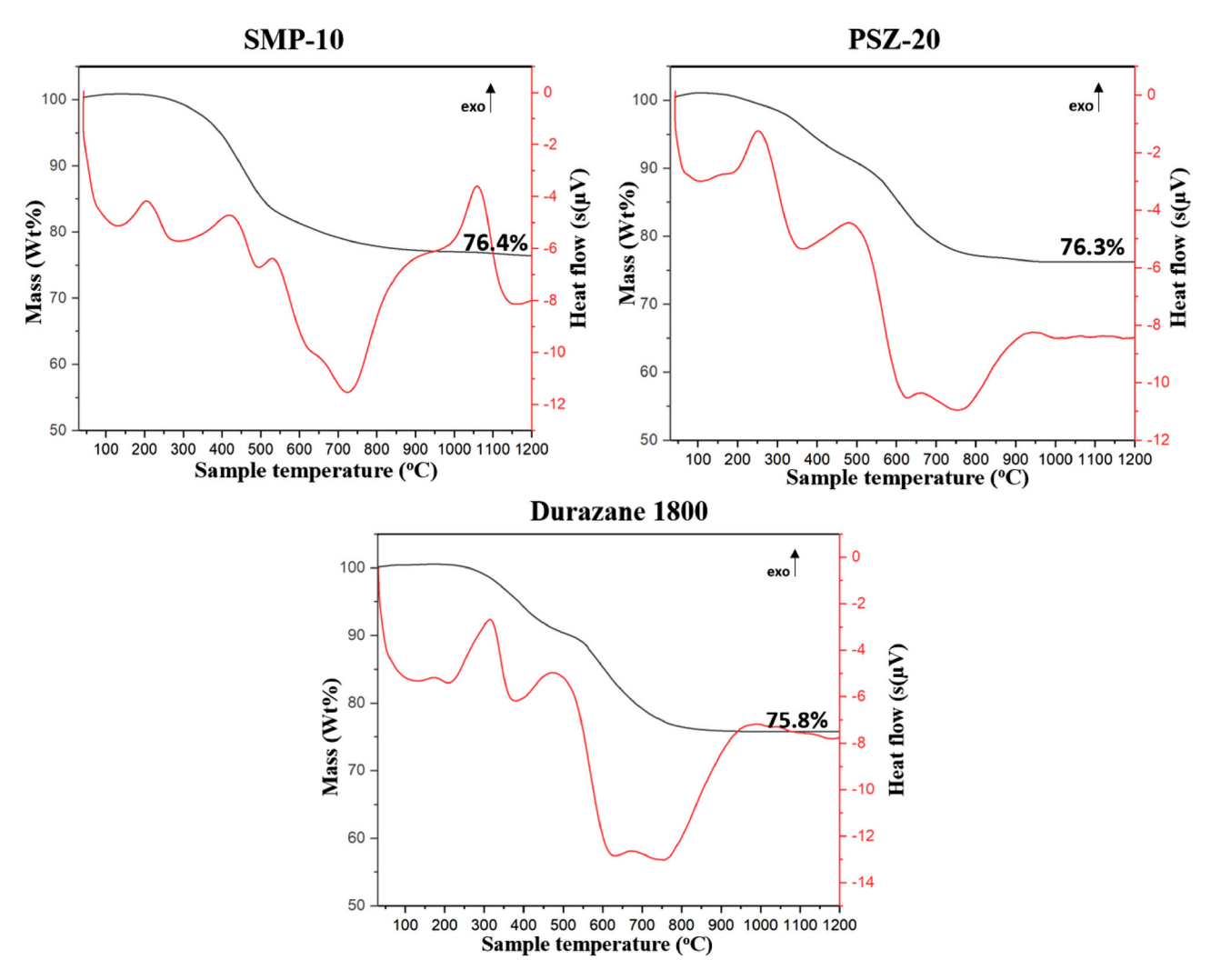


FIGURE 3 Thermogravimetric-differential scanning calorimetric (TG-DSC) curves of cross-linked precursors during pyrolysis (from ambient conditions to 1200°C), at ramp rate of 2°C/min, in flowing argon.

experiments are performed on all samples and results are shown in Figure 6.

The spectrum of the SiC(O) specimen derived from SMP-10 shown in Figure 6 is characterized by a relatively broad peak centered around -18 ppm that confirms presence of SiC domains and is consistent with poor crystallinity (The breadth of NMR peaks increases with loss of crystallinity).^{82,83} The NMR spectrum of SMP-10 does not suggest presence of significant amount of SiO₄ bonds, which contrasts results from XPS (discussed in the Section 3.1) and could suggest greater sensitivity of XPS to SiO₄ sites (or may indicate surface effects). The ²⁹Si MAS NMR spectra of samples derived from PSZ-20 and Durazane-1800 are characterized by a relatively broad signal centered around -30 ppm attributed to signature distribution of SiN_xC_{4-x} ($0 \le x \le 4$) units.⁸⁴ Appropriate peak fitting (with SiC_3N , SiC_2N_2 , $SiCN_3$, and SiN_4 signals at $\delta(^{29}Si) = -1$, -16, -32, and -49 ppm, respectively) permits identification of possible Si coordination number and bonding

environments. The integrated area under each NMR peak is proportional to the amount of each environment it represents within the microstructure.⁸⁵ As expected, the results in Figure 6 suggest presence of significant amounts of Si_3N_4 domains (from SiN_4 bonds) in the SiCN(O) PDCs. It appears that the samples have significant amounts of tetrahedrally coordinated Si in SiN₂C₂, SiN₃C, and SiN₄ environments, which are typical of localized mixed bonding domains in PDCs. 83,86 Mixed bonds can exist as isolated units, connected two or three dimensional networks or at the interface between domains (C, Si₃N₄, and SiC).^{79,83} The convolutions further suggest presence of only minor amounts of SiNC₃ mixed bonds in the samples. Overall, the relative amount of specific mixed bonds (from convolutions) appears to increase with greater N and less C per formula unit, as SiC_3N (~2%) < SiN_4 (~24%) < SiN_3C $(\sim 25\%) < SiN_2C_2 (\sim 40\%)$ (see Figure 6). The minor peak near ~-110 ppm is observed across all samples, which may indicate presence of SiO₄ species (~9% in SiCN(O)

15512916, 2023, 8, Downloaded from https://cer

nlinelibrary.wiley.com/doi/10.1111/jace.19153 by Kansas State University, Wiley Online Library on [18/10/2023]. See the Terms

on Wiley Online Library for rules of use; OA articles are governed by the applicable Creative Commons

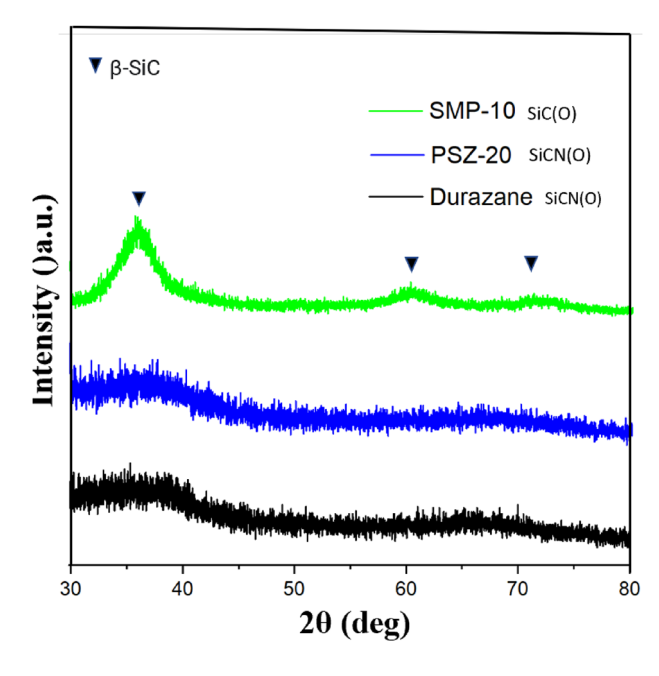


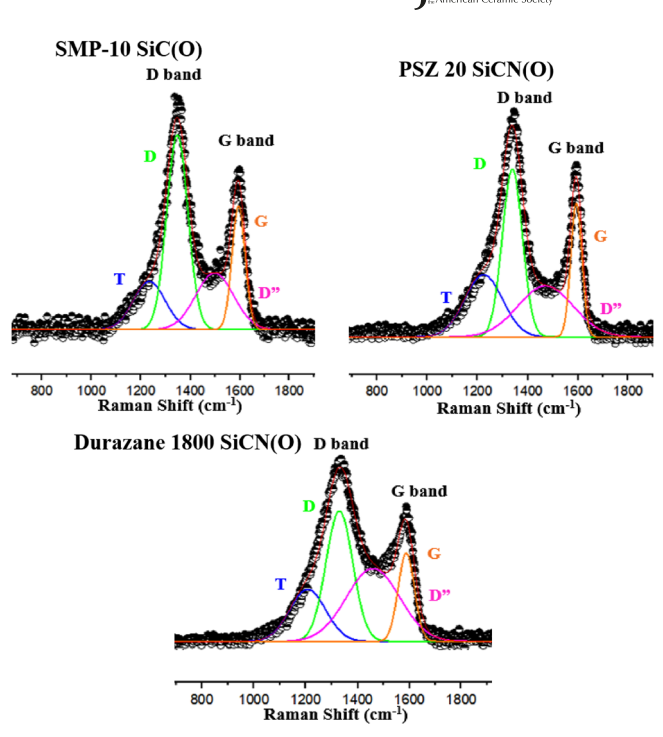
FIGURE 4 X-ray diffraction (XRD) patterns show growth of semicrystalline β -SiC in SiC(O) synthesized from SMP-10 at 1200°C. The SiCN(O) samples derived from PSZ-20 and Durazane-1800 are X-ray amorphous.

systems) in all the specimens, 86 and this is consistent with results from HR-XPS. The results do not suggest significant difference in the relative amounts of different SiN_rC_{4-r} bonds across the SiCN(O) specimens.

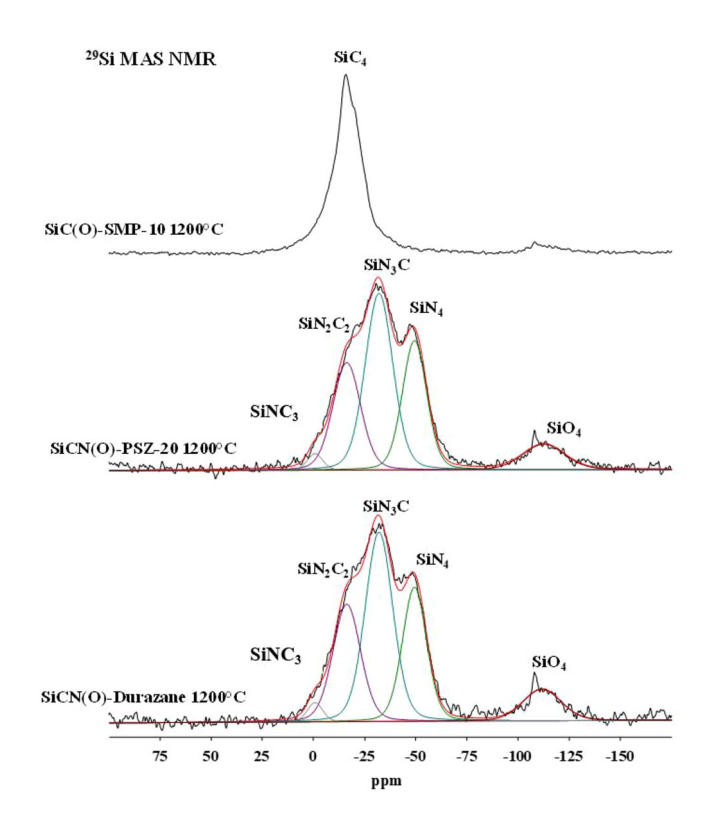
Typically, ²⁹Si CPMAS NMR can identify H termination in mixed bonding domains, especially in samples pyrolyzed at lower temperatures (H-rich samples).86 However, samples pyrolyzed above 1200°C typically have very low H content, which makes identification of Hterminated mixed bonds impractical.83

The bonding speciation in the microstructure of the PDCs can be identified by HR-XPS. The deconvolutions are obtained by performing appropriate curve fitting, and the area under the curve is proportional to the relative amount of corresponding bonding character. HR-XPS curves of the specimens are summarized in Figure 7. C 1s convolutions confirm presence of C-C (~285 eV), C-O (~289 eV), and C-N (~288.30 eV) bonds in the PDCs. 87-89 The presence of C-C bonds is consistent with results from Raman spectroscopy (see Figure 5) and may correspond to free carbon and/or C-C terminated mixed bonding domains. It is probable that C=O, C-O, and C-N convolutions correspond to bonding character in the free carbon phase.

The Si 2p deconvolutions identify presence of Si-C (\sim 101 eV), Si-O (\sim 103 eV), and SiO₄ (\sim 104 eV) bonds in all PDCs.^{89,90} The results further confirm presence of Si-N (~101.8 eV) bonds in the SiCN(O) specimens.⁸⁹ Typically, in mixed bonding, C is only bonded to Si or to another C. Therefore, SiO₄ bonds may correspond to



Raman spectra of polymer-derived ceramic (PDC) powders pyrolyzed at 1200°C.



²⁹Si MAS nuclear magnetic resonance (NMR) of FIGURE 6 SiC(O) derived SMP-10 as well as SiCN(O)s derived from PSZ-20 and Durazane-1800 at 1200°C, in flowing argon atmosphere.

15512916, 2023, 8, Downloaded from https://cer

onlinelibrary.wiley.com/doi/10.1111/jace.19153 by Kansas State University, Wiley Online Library on [18/10/2023]. See the Terms

on Wiley Online Library for rules of use; OA articles are governed by the applicable Creative Commons License)

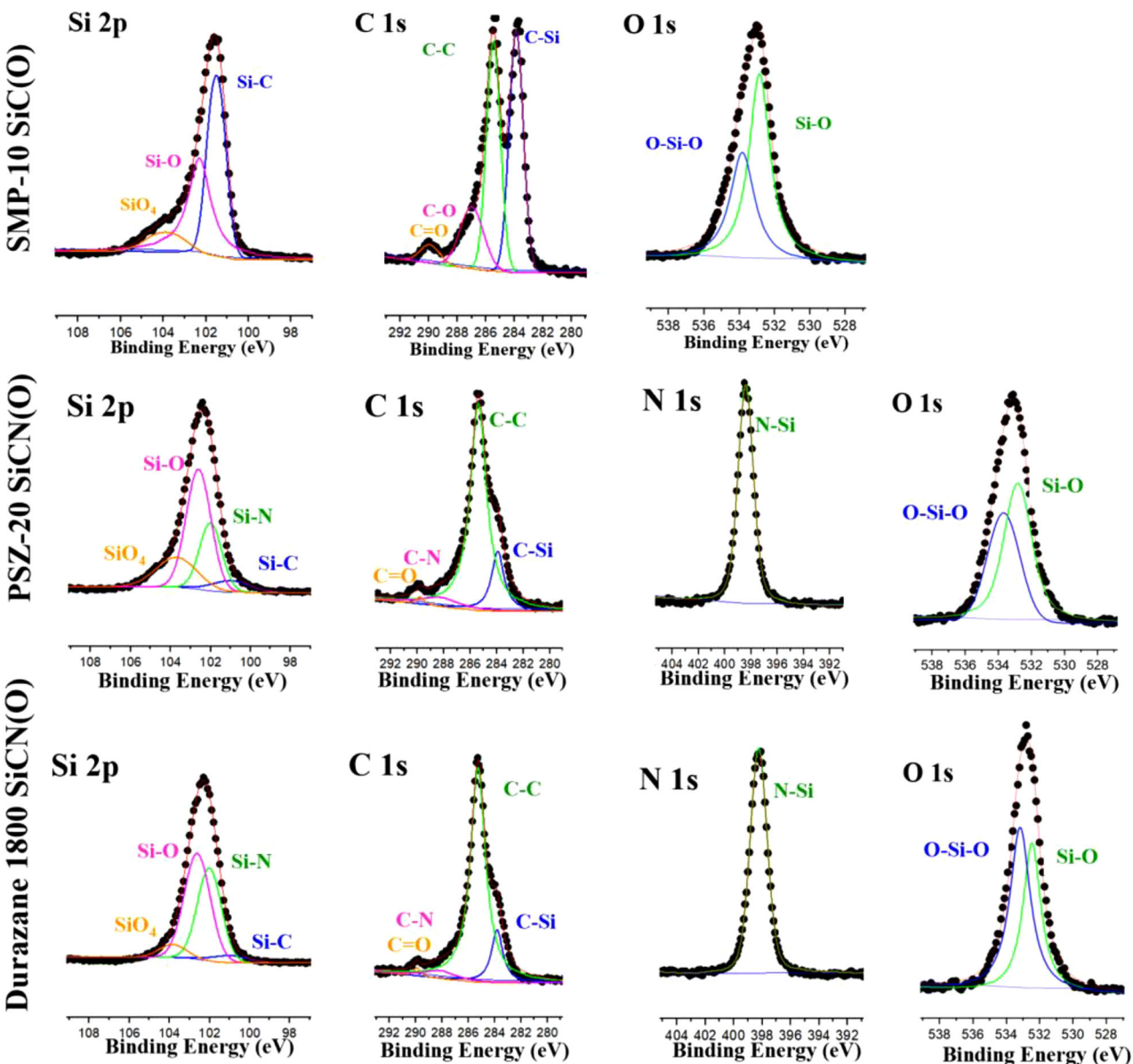


FIGURE 7 High-resolution X-ray photoemission spectroscopy (HR XPS) of SiC(O) and SiCN(O) polymer-derived ceramics (PDCs) derived from SMP-10, PSZ-20, and Durazane-1800.

formation of amorphous silica (SiO_2) domains. Only a small portion of Si–C and Si–O convolutions are expected to represent SiO_xC_{4-x} mixed bonding networks in the microstructure of the PDCs, as their respective NMR peaks are not observed (see Figure 6). It is likely that Si–C and Si–O bonds mostly include contributions from SiC (silicon carbide) and SiO_2 amorphous domains, respectively. Unfortunately, the Si–O and Si–C bonds from mixed bonds cannot be differentiated from those present in the corresponding stoichiometric domains. Additionally, Si–N bonds may represent formation of amorphous Si_3N_4 and/or SiN_xC_{4-x} mixed bonding domains. The results in

Figure 7 may indicate that the SiC(O) sample contains larger relative amount of SiC domains (from Si–C convolutions) compared to SiCN(O)s. It is also apparent that SiCN(O) derived from Durazane-1800 displays greatest amounts (relative to Si–O bonds) of $\mathrm{Si}_3\mathrm{N}_4$ and/or $\mathrm{SiN}_x\mathrm{C}_{4-x}$ mixed bonding domains compared to the SiCN(O) specimen derived from PSZ-20. It should be noted that C 1s spectra suggest only minor amounts of N bonded to C in SiCN(O) samples, and this may imply that there are two chemical states in N 1s, specifically, N–Si and N–C. However, the sharp peak in the N 1s spectra of SiCN(O)s suggests negligible amounts of N–C relative to N–Si bonds.

15512916, 2023, 8, Downloaded from https://ceramics.onlinelibrary.wiley.com/doi/10.1111/jace.19153 by Kansas State University, Wiley Online Library on [18/10/2023]. See the Terms and Conditions (https://onlinelibrary.wiley.com/term

and-conditions) on Wiley Online Library for rules of use; OA articles are governed by the applicable Creative Commons License

Journal

Elemental analysis of SiOC samples from X-ray photoemission spectroscopy (XPS) survey scan.

Elements (at.%)							
SiC(N)(O)	Pyrolysis	Ideal PDC					C _{free} /C
precursor	temperature (°C)	system	C	N	0	Si	(%)
SMP-10	1200	SiC	48.24	-	17.90	33.85	40
PSZ-20	1200	SiC(N)	33.50	15.77	15.51	35.22	74.74
Durazane-1800	1200	SiC(N)	34.63	16.63	12.77	35.97	78.32

Note: Cfree/C is determined from C 1s convolutions, by assuming that all C-C bonds are part of free carbon phase, and not mixed bonds. Abbreviation: PDC, polymer-derived ceramic.

This would be consistent with scarce N-termination in the free carbon phase, relative to stoichiometric domains and mixed bonds.

3.1 Elemental analysis

Thermochemical calculations of enthalpies of formation require well characterized compositions. XPS is an efficient tool for characterization of PDCs pyrolyzed at high temperatures, when H from residual organics is scarce. In this work, we employ XPS (Si 2p, C1s, O1s, and N1s) survey scans for quantitation of Si, C, N, and O content in the samples. The results from survey scans confirm significant Si, C, and O content in all samples, and additional N is present in the microstructure of SiCN(O) PDCs. The calculated phase assemblages suggest greater relative amount of free carbon in the SiC(O) compared to SiCN(O) ceramics. The results are summarized in Table 5. There are similarities in compositions derived from PSZ-20 and Durazane-1800. The minor compositional differences may result from dissimilarities in curing temperature and the ratio of Si-vinyl to Si-methyl groups in the oligomers.

3.2 | Systematics of thermodynamic stabilization in PDCs

The discussion that follows addresses thermodynamic stabilization in SiOC and SiOCN ceramic systems. Samples derived from the industrial precursors (PSZ-20, SMP-10, and Durazane-1800) permit investigation of SiOCN compositions outside the range of structures previously explored by high temperature calorimetry. These data are valuable additions to the thermodynamic database of PDCs previously investigated. The results validate past knowledge on structure-stability trends in PDCs and further suggest possible systematic differences in the stabilizing effect of different mixed bonding environments (oxygen or nitrogen). Additionally, this work identifies trends/correlations between elemental content (composition) and thermodynamic stability of the ceramics.

The results from thermodynamic analysis are summarized in Table 6. The enthalpies of dissolution (ΔH°_{dis}) are most exothermic for the SiC(O) sample. This results from highly exothermic enthalpies for the oxidation of greater amounts of C and Si and has been seen in previous studies. 58,77,86 Enthalpies of formation permit quantitation of relative thermodynamic stabilities. The results in Table 6 show that enthalpies of formation from elements $(\Delta H^{\circ}_{f, elem})$ are most exothermic for SiCN(O) PDCs compared to the SiC(O) specimen. The enthalpies of formation from elements include the energetics for forming stoichiometric compounds (SiO₂, SiC, and Si₃N₄) from the elements and are more exothermic than the enthalpy of formation from those crystalline components. The entropy of formation from elements has a negative (destabilizing) contribution arising from confining N2 and O2 gas into stoichiometric solids. However, the highly exothermic enthalpies of formation from elements overcome the entropy effect and stabilize the structures. Considering the enthalpy of formation of the $Si_aO_bC_cN_d$ specimens from binary crystalline components SiO2, SiC, and Si3N4 $(\Delta H^{\circ}_{f, comp})$ allows one to focus on the interdomain interactions in the microstructure. Across all structures studied by calorimetry, each with a different composition, enthalpies from components range from -128 to +20 kJ/mol (see Table 7), note that results in Table 7 are in terms of per one mol of Si (kJ/mol Si). 46,58,91-93 As PDCs are amorphous, their entropies of formation from crystalline components are expected to be positive, arising from disorder. Such positive entropy effects add to the stabilization relative to binary crystalline components. Thus, most PDCs have negative free energies of formation from the binary crystalline components and are thermodynamically stable with respect to an isocompositional mixture of these components and would not decompose to them. However, decomposition because of carbothermal reduction (under reducing conditions) or oxide formation (under oxidizing conditions) limits their stability at high temperature. Structural and chemical characterization in this study point to notable differences in the chemistry and structure of SiC(O) compared to the SCN(O), as expected. The microstructural modifications result in significant



TABLE 6 Summary of enthalpies of dissolution (ΔH°_{dis}), enthalpies of formation from elements ($\Delta H^{\circ}_{f, elem}$), and enthalpies of formation from components ($\Delta H^{\circ}_{f, comp}$), of samples derived from industrial precursors.

Sample	Composition $Si_aO_bC_cN_d$ (a+b+c+d=1)	$\Delta H^{\circ}_{ m dis}$ (kJ/mol)	$\Delta H^{\circ}_{ m f,elem}$ (kJ/mol)	$\Delta H^{\circ}_{ m f,comp}$ (kJ/mol)
SMP-10	$Si_{0.34}O_{0.18}C_{0.48}$	-461.12 ± 4.12	-20 ± 4.63	80.12 ± 4.65
PSZ-20	$Si_{0.35}O_{0.16}C_{0.33}N_{0.16}$	-352.51 ± 0.98	-78.55 ± 2.32	33.89 ± 4.66
Durazane-1800	$Si_{0.36}O_{0.13}C_{0.35}N_{0.17}$	-362.31 ± 0.56	-85.09 ± 2.18	21.4 ± 4.58

TABLE 7 Summary of enthalpies of formation of amorphous SiOC and SiOCN polymer-derived ceramics (PDCs), synthesized between 800 and 1200°C.

Sample name (as referred in the cited literature)	а	b	с	d	e	Pyrolysis temperature (°C)	$\Delta H^{\circ}_{\mathrm{f, comp}}$ (kJ/mol of Si)
S1	0.364	0.513	0.123	0	0	1200	-54.4^{94}
S2	0.295	0.44	0.265	0	0	1200	-24.7^{94}
S3	0.271	0.374	0.355	0	0	1200	-126.2^{94}
S4	0.278	0.278	0.444	0	0	1200	-64.0^{94}
S5	0.259	0.238	0.503	0	0	1200	-495.0^{94}
W1B	0.35	0.42	0.231	0	0	1200	-78.8^{95}
W2B	0.364	0.378	0.258	0	0	1200	-111.0^{95}
W3B	0.299	0.311	0.386	0	0	1200	-111.7^{95}
W4B	0.235	0.209	0.556	0	0	1200	-65.9^{95}
SiOC	0.314	0.467	0.22	0	0	1200	-68.5^{96}
S1200	0.307	0.461	0.232	0	0	1200	-16.0^{97}
CS1200	0.085	0.144	0.771	0	0	1200	84.197
Si	0.345	0.523	0.088	0.044	0	1200	-60.9^{96}
PhSiO _{1.5} _SG	0.112	0.227	0.47	0.191	0	800	-22.3^{58}
HQ4_SG	0.283	0.588	0.078	0.052	0	1100	-11.3^{58}
PhSiO _{1.5} _SG	0.142	0.23	0.568	0.06	0	1100	-97.9^{58}
SiOC	0.313	0.473	0.213	0	0	1100	-48.5^{98}
GM35	0.096	0.041	0.346	0.273	0.244	800	-441.7^{86}
GM35	0.134	0.015	0.435	0.13	0.285	1100	-192.5^{86}
HN1	0.121	0.02	0.594	0.119	0.149	800	-264.5^{86}
HN1	0.126	0.019	0.671	0.034	0.151	1100	-205.5^{86}
S3	0.204	0	0.556	0	0.239	1100	-13.7^{78}
Black	0.318	0.485	0.192	0.005	0	1100	-13^{99}

Note: This data summarize thermochemical analysis of some compositions previously investigated by high temperature calorimetry. The enthalpies are in terms of per one mol of Si.

difference in the thermodynamic drive for the formation of their corresponding structures (see Table 6). This permits identification of the influence of chemical species (Si, C, O, or N) on structure and stability. The results in Table 6 suggest that SiC(N)(O) structures, with alloyed amounts of both O and N (N/O < 2) can be more stable than SiC(O) specimens. Previous studies on PDC fibers and powders also point to greater stability of SiOCN samples with

alloyed amounts of O and N species in the structure. 46,92 The increased stabilization likely results from inclusion of both SiN_xC_{4-x} and SiO_xC_{4-x} mixed bonds in the PDCs.

An important factor in the thermodynamic stabilization of PDC structures includes mixed bonding which can occur at the interface of stoichiometric domains ($\mathrm{Si_3N_4}$, $\mathrm{SiO_2}$, C, and SiC). Previous investigations show that more mixed bonding can stabilize structures by as much as

20 kJ/mol. Nonetheless, there is still a lingering question whether SiN_xC_{4-x} and SiO_xC_{4-x} mixed bonds differ significantly in their stabilizing effect. In this work, the Si 2p convolutions and NMR spectra confirm presence of significant amounts of SiN_xC_{4-x} mixed bonds in SiCN(O) specimens, but not in the SiC(O) derived from SMP-10. There is systematic thermodynamic stabilization of the PDCs with addition of SiN_xC_{4-x} bonds, as Table 6 highlights the lower thermodynamic stability of the SiC(O) specimen. This indicates significant (~60 kJ/mol) enthalpic stabilization from addition of SiN_xC_{4-x} mixed bonds to SiC(O) systems, which is ~10 kJ/ mol higher than stabilization from addition of SiO_xC_{4-x} mixed bonds to SiC PDC fibers. 46 Furthermore, Si 2p XPS convolutions of the SiCN(O) samples (see Table 6) also suggest the greatest relative amount of SiO₂ and/or SiO_xC_{4-x} (from Si-O bonds) as well as the lowest amount of Si_3N_4 and/or SiN_xC_{4-x} mixed bonds (from Si-N bonds) in the SiCN(O) derived from PSZ-20 (compared to Durazane-1800). The enthalpies of formation in Table 6 highlight the lower stability of the SiCN(O) structure derived from PSZ-20 (compared to Durazane-1800). Overall, the results may indicate a greater stabilizing effect from SiN_xC_{4-x} compared to SiO_xC_{4-x} mixed bonds. This could imply significant stabilization of quaternary SiOCN structures by tuning the ratio of SiO_xC_{4-x} to SiN_xC_{4-x} mixed bonds. It is likely that there exists an optimum ratio that promotes greatest stability.

The SiCN(O) specimens in Table 6 are outside the compositional range of structures previously studied. This permits assessment of systematics in the correlation between elemental content and thermodynamic stability in PDCs. This is important since only few studies explored enthalpic stabilization in quaternary SiCN(O) structures (see Figure 8a,b). Overall, the results in Figure 8a,b point to increased stabilization relative to binary crystalline components of quaternary SiOCN systems with decrease in Si and O content. In contrast, greater O content appears to destabilize ternary SiOC systems (see Figure 8c,d). In both systems (SiOC and SiOCN), destabilization at higher Si content may reach a plateau, which could imply only minor/negligible further destabilization of the structures with much higher Si content (see Figure 8a,c). The effect of O content on thermodynamic stability (see Figure 8b,d) may reach a plateau as well. No obvious correlation is observed between enthalpy of formation and C content. The results show that the addition of significant amounts of N species to SiOC structures can significantly impact the systematic trend for increased stabilization in the ceramics. This implies that the correlations are system dependent (SiOC or SiCNO). The semicrystalline structure of the SiC(O) specimen (confirmed from XRD) may contribute to its more positive enthalpy of formation,

compared to the other amorphous samples synthesized at 1200°C (Figure 8c,d).

The effect of synthesis temperature is an important factor to be considered in the thermodynamic stabilization of PDCs; however, in this current work we constrain the synthesis temperature to 1200°C due to equipment limitations. Typically, there are microstructural modifications associated with pyrolysis time and temperature. 58,76,93,96 The accumulated thermochemical data indicate overall increase in the thermodynamic stability of PDCs with increasing pyrolysis temperature (800–1450°C). 95,96 Some samples synthesized at intermediate temperature (1200°C) are energetically less stable than specimens synthesized at lower (800-1000°C) and higher (1400°C) temperatures. 95,96 Such lower stability may reflect decrease of H-terminated mixed bonds, due to evolution of residual (H) up to ~1200°C, as previously reported.⁷⁹ This highlights the significant stabilizing effect of H termination in low-temperature samples, especially those containing nitrogen. It is expected that the SiCN(O) quaternary systems would display a temperature-stability trend similar to that of SiOC and SiCN parent structures, as previous works indicate.⁸⁶ However, several fundamental questions still remain. Does the stability of PDCs depend on porosity, and if so, how? How does the stabilizing effect of different metal fillers depend on ionic radius and/or electronegativity of the metal, and is it temperature dependent? How do ionic radius, electronegativity and other metal descriptors influence, temperature-stability relation, including thermodynamic resistance to carbothermal reduction and crystallization in PDCs. To what extent do such trends differ for SiOC, SiCN, and SiOCN systems? What factors, thermodynamic and/or kinetic limit the compositions at which PDCs can be made? Thus, much systematic work still remains to be done. Future investigations require more thermodynamic measurements and perhaps the use of softwares like CALPHAD to compare with experimental data and predict thermodynamic properties of multicomponent PDC systems. 100,101

CONCLUSIONS

In this study, we measured the energetics of SiC(O) and SiCN(O) PDC compositions derived from industrial preceramic polymers. The structure-stability trends are consistent with the current understanding of thermodynamic stabilization in PDCs observed across other structures derived from both commercial and other tailor-made precursors. Overall, the thermodynamic stability of the quaternary SiCN(O) PDCs increases with increase in N content and decrease in the relative amount of O. New

15512916, 2023, 8, Downloaded from https://ceramic

onlinelibrary.wiley.com/doi/10.1111/jace.19153 by Kansas State University, Wiley Online Library on [18/10/2023]. See the Terms

ns) on Wiley Online Library for rules of use; OA articles are governed by the applicable Creative Commons Licenso

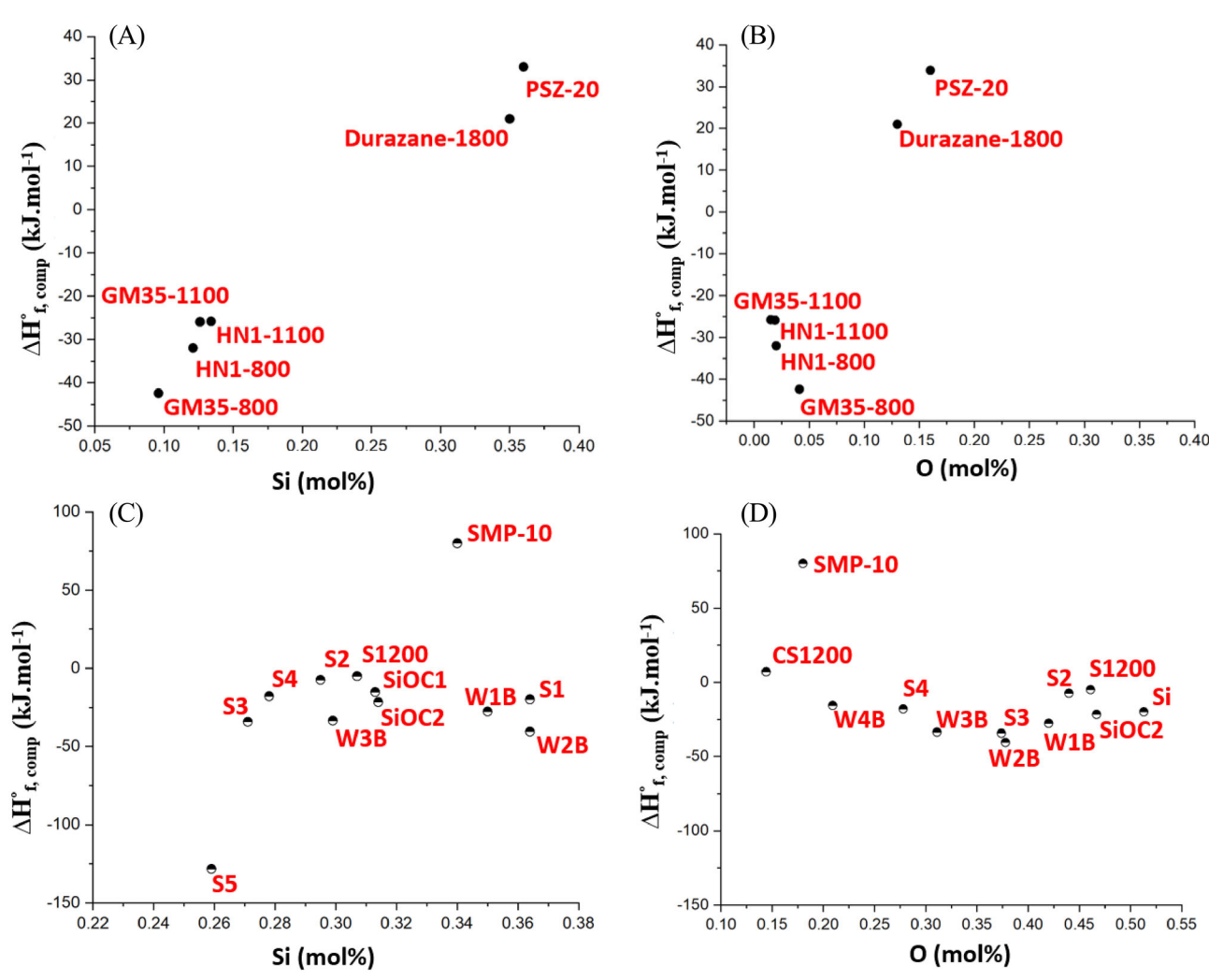


FIGURE 8 Correlation between enthalpy of formation of SiOCN structures as function of (A) Si and (B) O content. Enthalpy of formation of SiOC polymer-derived ceramics (PDCs) synthesized at 1200°C as function of (C) Si and (D) O content. This includes data from Refs. [79, 88, 89, 91] in Table 7.

observations suggest greater stabilizing effect of $\mathrm{SiN}_x\mathrm{C}_{4-x}$ compared to $\mathrm{SiO}_x\mathrm{C}_{4-x}$ mixed bonds. This study poses new questions for the rigorous understanding of thermodynamic stabilization in PDCs. This is important in understanding the effect of composition and microstructure (independent of synthesis method) on the thermodynamic drive for phase separation and decomposition (into binary carbides, oxides, and nitrides) in amorphous ceramics structures, including CMCs developed by PIP technique.

ACKNOWLEDGMENTS

Financial support from National Science Foundation (NSF) Partnerships for International Research and Education (PIRE) grant #1743701 is gratefully acknowledged. The polymeric precursors were provided by PIRE partner, Dr. Zlatomir Apostolov.

ORCID

Alexandra Navrotsky https://orcid.org/0000-0002-3260-

REFERENCES

- Luo X, Wang J, Dooner M, Clarke J. Overview of current development in electrical energy storage technologies and the application potential in power system operation. Appl Energy. 2015;137:511–36.
- 2. Eswarappa Prameela S, Pollock TM, Raabe D, Meyers MA, Aitkaliyeva A, Chintersingh K-L, et al. Materials for extreme environments. Nat Rev Mater. 2023;8:81–8.
- Jia Y, Ajayi TD, Roberts MAJ, Chung C-C, Xu C. Ultrahightemperature ceramic-polymer-derived SiOC ceramic composites for high-performance electromagnetic interference shielding. ACS Appl Mater Interfaces. 2020;12(41):46254-66.
- 4. Chauhan SS, Abraham M, Choudhary V. Superior EMI shielding performance of thermally stable carbon

- nanofiber/poly(ether-ketone) composites in 26.5–40 GHz frequency range. J Mater Sci. 2016;51(21):9705–15.
- 5. Hamerton I, Mooring L. 7 The use of thermosets in aerospace applications. In: Guo Q, editor. Thermosets. Sawston: Woodhead Publishing; 2012. p. 189–227.
- Iqbal A, Saeed A, Ul-Hamid A. A review featuring the fundamentals and advancements of polymer/CNT nanocomposite application in aerospace industry. Polym Bull. 2021;78(1):539– 57.
- Jia Y, Ajayi TD, Morales J, Chowdhury AR, Sauti G, Chu S-H, et al. Thermal properties of polymer-derived ceramic reinforced with boron nitride nanotubes. J Am Ceram Soc. 2019;102(12):7584–93.
- Liu C, Zhang L, Li X, Chang X, Wu Y, Wang X. Synthesis, characterization, and ceramization of a carbon-rich SiCw-ZrC-ZrB₂ preceramic polymer precursor. Ceram Int. 2019;45(13):16097–104.
- Xie Z, Deng X, Suo X, Zhou T, Gou Y. Synthesis and characterization of zirconium diboride precursor based on polycentric bridge bonds. Mater Chem Phys. 2015;159:178–84.
- Mansfield B, Torres S, Yu T, Wu D. A review on additive manufacturing of ceramics. ASME Digital Collection. 2019;1:2886–98.
- Parikh PB. Alumina ceramics: engineering applications and domestic market potential. Trans Indian Ceram Soc. 1995;54(5):179–84.
- 12. Chaudhary RP, Parameswaran C, Idrees M, Rasaki AS, Liu C, Chen Z, et al. Additive manufacturing of polymer-derived ceramics: materials, technologies, properties and potential applications. Prog Mater Sci. 2022;128:100969.
- 13. Wei GC. Beta SiC powders produced by carbothermic reduction of silica in a high-temperature rotary furnace. J Am Ceram Soc. 1983;66(7):c111–3.
- 14. Moshtaghioun BM, Poyato R, Cumbrera FL, de Bernardi-Martin S, Monshi A, Abbasi MH, et al. Rapid carbothermic synthesis of silicon carbide nano powders by using microwave heating. J Eur Ceram Soc. 2012;32(8):1787–94.
- Carassiti L, Jones A, Harrison P, Dobson PS, Kingman S, MacLaren I, et al. Ultra-rapid, sustainable and selective synthesis of silicon carbide powders and nanomaterials via microwave heating. Energy Environ Sci. 2011;4(4):1503– 10
- Zhao W, Shao G, Jiang M, Zhao B, Wang H, Chen D, et al. Ultralight polymer-derived ceramic aerogels with wide bandwidth and effective electromagnetic absorption properties. J Eur Ceram Soc. 2017;37(13):3973–80.
- Salles V, Bernard S, Brioude A, Cornu D, Miele P. A new class of boron nitride fibers with tunable properties by combining an electrospinning process and the polymer-derived ceramics route. Nanoscale. 2010;2(2):215-7.
- Prasad RM, Mera G, Morita K, Müller M, Kleebe H-J, Gurlo A, et al. Thermal decomposition of carbon-rich polymer-derived silicon carbonitrides leading to ceramics with high specific surface area and tunable micro- and mesoporosity. J Eur Ceram Soc. 2012;32(2):477–84.
- 19. Wang B, Song Y, Zhang X, Chen K, Liu M, Hu X, et al. Polymer derived SiBCN(O) ceramics with tunable element content. Ceram Int. 2022;48(7):10280–7.

- 20. Mazo MA, Tamayo A, Caballero AC, Rubio J. Electrical and thermal response of silicon oxycarbide materials obtained by spark plasma sintering. J Eur Ceram Soc. 2017;37(5):2011–20.
- 21. Yu S, Tu R, Goto T. Preparation of SiOC nanocomposite films by laser chemical vapor deposition. J Eur Ceram Soc. 2016;36(3):403–9.
- Vasudev MC, Anderson KD, Bunning TJ, Tsukruk VV, Naik RR. Exploration of plasma-enhanced chemical vapor deposition as a method for thin-film fabrication with biological applications. ACS Appl Mater Interfaces. 2013;5(10):3983–94.
- Rajagopalan T, Wang X, Lahlouh B, Ramkumar C, Dutta P, Gangopadhyay S. Low temperature deposition of nanocrystalline silicon carbide films by plasma enhanced chemical vapor deposition and their structural and optical characterization. J Appl Phys. 2003;94(8):5252–60.
- Jonas S, Ptak WS, Sadowski W, Walasek E, Paluszkiewicz C. FTIR in situ studies of the gas phase reactions in chemical vapor deposition of SiC. J Electrochem Soc. 1995;142(7):2357.
- Vakifahmetoglu C, Zeydanli D, Colombo P. Porous polymer derived ceramics. Mater Sci Eng. R: Rep. 2016;106:1–30.
- Zhou S, Mei H, Chang P, Lu M, Cheng L. Molecule editable 3D printed polymer-derived ceramics. Coord Chem Rev. 2020;422:213486.
- Colombo P. Engineering porosity in polymer-derived ceramics.
 J Eur Ceram Soc. 2008;28(7):1389–95.
- 28. Lei Y, Wang Y, Song Y, Deng C. Novel processable precursor for BN by the polymer-derived ceramics route. Ceram Int. 2011;37(8):3005–9.
- Mera G, Gallei M, Bernard S, Ionescu E. Ceramic nanocomposites from tailor-made preceramic polymers. Nanomaterials. 2015;5(2):468–540.
- Colombo P, Mera G, Riedel R, Sorarù GD. Polymer-derived ceramics: 40 years of research and innovation in advanced ceramics. J Am Ceram Soc. 2010;93(7):1805–37.
- 31. Goerke O, Feike E, Heine T, Trampert A, Schubert H. Ceramic coatings processed by spraying of siloxane precursors (polymerspraying). J Eur Ceram Soc. 2004;24(7):2141–7.
- 32. Greil P. Polymer derived engineering ceramics. Adv Eng Mater. 2000;2(6):339–48.
- Lücke J, Hacker J, Suttor D, Ziegler G. Synthesis and characterization of silazane-based polymers as precursors for ceramic matrix composites. Appl Organomet Chem. 1997;11(2):181–94.
- Hurwitz FI. Filler/polycarbosilane systems as CMC matrix precursors. In: 22nd Annu. Conf. Compos. Adv. Ceram. Mater. Struct. Ceram. Eng. Sci. Proc. John Wiley & Sons, Ltd; 1988. p. 267–74.
- Grossenbacher J, Gullo MR, Grandjean R, Kiefer T, Brugger J. Sub micrometer ceramic structures fabricated by molding a polymer-derived ceramic. Microelectron Eng. 2012;97:272–5.
- Ren Z, Gervais C, Singh G. Fabrication and characterization of silicon oxycarbide fibre-mats via electrospinning for high temperature applications. RSC Adv. 2020;10(63):38446–55.
- Mujib SB, Cuccato R, Mukherjee S, Franchin G, Colombo P, Singh G. Electrospun SiOC ceramic fiber mats as freestanding electrodes for electrochemical energy storage applications. Ceram Int. 2020;46(3):3565–73.
- 38. Chen Z, Li Z, Li J, Liu C, Lao C, Fu Y, et al. 3D printing of ceramics: a review. J Eur Ceram Soc. 2019;39(4):661–87.



- Zhao L, Wang X, Xiong H, Zhou K, Zhang D. Optimized preceramic polymer for 3D structured ceramics via fused deposition modeling. J Eur Ceram Soc. 2021;41(10):5066–74.
- 40. Chen H, Wang X, Xue F, Huang Y, Zhou K, Zhang D. 3D printing of SiC ceramic: direct ink writing with a solution of preceramic polymers. J Eur Ceram Soc. 2018;38(16):5294–300.
- Schiavon MA, Gervais C, Babonneau F, Soraru GD. Crystallization behavior of novel silicon boron oxycarbide glasses. J Am Ceram Soc. 2004;87(2):203–8.
- Ionescu E, Kleebe H-J, Riedel R. Silicon-containing polymerderived ceramic nanocomposites (PDC-NCs): preparative approaches and properties. Chem Soc Rev. 2012;41(15):5032–52.
- Tavakoli AH, Gerstel P, Golczewski JA, Bill J. Effect of boron on the crystallization of amorphous Si-(B-)C-N polymer-derived ceramics. J Non-Cryst Solids. 2009;355(48):2381-9.
- 44. Terauds K, Raj R. Limits to the stability of the amorphous nature of polymer-derived HfSiCNO compounds. J Am Ceram Soc. 2013;96(7):2117–23.
- Kleebe H-J, Suttor D, Müller H, Ziegler G. Decompositioncrystallization of polymer-derived Si-C-N ceramics. J Am Ceram Soc. 1998;81(11):2971–7.
- Leonel GJ, Mujib SB, Singh G, Navrotsky A. Thermodynamic stabilization of crystalline silicon carbide polymer-derived ceramic fibers. Int J Ceram Eng Sci. 2022;4(5):315–26.
- 47. Soraru GD, Babonneau F, Mackenzie JD. Structural evolutions from polycarbosilane to SiC ceramic. J Mater Sci. 1990;25(9):3886–93.
- Nazari KA, Tran P, Tan P, Ghazlan A, Ngo TD, Min Xie Y. Preceramic polymer composite: fabrication process and mechanical performance. Mater Lett. 2022;318:132218.
- Nabat Al-Ajrash SM, Browning C, Eckerle R, Cao L. Initial development of preceramic polymer formulations for additive manufacturing. Mater Adv. 2021;2(3):1083–9.
- Jana P, Santoliquido O, Ortona A, Colombo P, Sorarù GD. Polymer-derived SiCN cellular structures from replica of 3D printed lattices. J Am Ceram Soc. 2018;101(7):2732–8.
- 51. Apostolov ZD, Heckman EP, Key TS, Cinibulk MK. Effects of low-temperature treatment on the properties of commercial preceramic polymers. J Eur Ceram Soc. 2020;40(8):2887–95.
- 52. Colombo P. Polymer derived ceramics: from nano-structure to applications. Lancaster: DEStech Publications, Inc.; 2010.
- Lale A, Schmidt M, Mallmann MD, Bezerra AVA, Diz Acosta E, Machado RAF, et al. Polymer-derived ceramics with engineered mesoporosity: from design to application in catalysis. Surf Coat Technol. 2018;350:569–86.
- 54. Bernard S, Fiaty K, Cornu D, Miele P, Laurent P. Kinetic modeling of the polymer-derived ceramics route: investigation of the thermal decomposition kinetics of poly[B-(methylamino)borazine] precursors into boron nitride. J Phys Chem B. 2006;110(18):9048–60.
- 55. Key TS, Patel DK, Wilks GB, Cinibulk MK. Modeling the pyrolysis of preceramic polymers: a kinetic study of the polycarbosilane SMP-10. J Eur Ceram Soc. 2021;41(13):6356–65.
- 56. Key TS, Wilks GB, Parthasarathy TA, King DS, Apostolov ZD, Cinibulk MK. Process modeling of the low-temperature evolution and yield of polycarbosilanes for ceramic matrix composites. J Am Ceram Soc. 2018;101(7): 2809–18.

- Massiot D, Fayon F, Capron M, King I, Le Calvé S, Alonso B, et al. Modelling one- and two-dimensional solid-state NMR spectra. Magn Reson Chem. 2002;40(1):70–6.
- Sugie C, Navrotsky A, Lauterbach S, Kleebe H-J, Mera G. Structure and thermodynamics of silicon oxycarbide polymerderived ceramics with and without mixed-bonding. Materials. 2021;14(15):4075.
- Navrotsky A. Progress and new directions in calorimetry: a 2014 perspective. J Am Ceram Soc. 2014;97(11):3349–59.
- Deepa M, Sharma N, Agnihotry SA, Chandra R. FTIR investigations on ion-ion interactions in liquid and gel polymeric electrolytes: LiCF₃SO₃-PC-PMMA. J Mater Sci. 2002;37(9):1759–65.
- Zhang GY, Peak D. Studies of Cd(II)–sulfate interactions at the goethite–water interface by ATR-FTIR spectroscopy. Geochim Cosmochim Acta. 2007;71(9):2158–69.
- Bruzzoniti MC, Appendini M, Rivoira L, Onida B, Del Bubba M, Jana P, et al. Polymer-derived ceramic aerogels as sorbent materials for the removal of organic dyes from aqueous solutions. J Am Ceram Soc. 2018:101(2):821–30.
- Bin Mujib S, Ribot F, Gervais C, Singh G. Self-supporting carbon-rich SiOC ceramic electrodes for lithium-ion batteries and aqueous supercapacitors. RSC Adv. 2021;11(56):35440–54.
- 64. Santhosh B, Vakifahmetoglu C, Ionescu E, Reitz A, Albert B, Sorarù GD. Processing and thermal characterization of polymer derived SiCN(O) and SiOC reticulated foams. Ceram Int. 2020;46(5):5594–601.
- 65. Zhao W, Shao G, Han S, Cai C, Liu X, Sun M, et al. Facile preparation of ultralight polymer-derived SiOCN ceramic aerogels with hierarchical pore structure. J Am Ceram Soc. 2019;102(5):2316–24.
- 66. Li H, Zhang L, Cheng L, Wang Y, Yu Z, Huang M, et al. Polymer–ceramic conversion of a highly branched liquid polycarbosilane for SiC-based ceramics. J Mater Sci. 2008;43(8):2806–11.
- Mahmoudi M, Kim S, Arifuzzaman AM, Saito T, Cramer CL, Minary-Jolandan M. Processing and 3D printing of SiCN polymer-derived ceramics. Int J Appl Ceram Technol. 2022;19(2):939–48.
- Li M, Cheng L, Ye F, Wang Y, Zhang C. Tailoring dielectric properties of PDCs-SiCN with bimodal pore-structure by annealing combined with oxidation. J Eur Ceram Soc. 2020;40(15):5247–57.
- Liu X, Xue J, Ren F, Ye F, Fan X, Liu Y, et al. Enhanced microwave-absorption properties of polymer-derived SiC/SiOC composite ceramics modified by carbon nanowires. Ceram Int. 2020;46(13):20742–50.
- Hung I, Ionescu E, Sen J, Gan Z, Sen S. Structure and connectivity in an amorphous silicon oxycarbide polymer-derived ceramic: results from 2D ²⁹Si NMR spectroscopy. J Phys Chem C. 2021;125(8):4777–84.
- 71. Saha A, Raj R. Crystallization maps for SiCO amorphous ceramics. J Am Ceram Soc. 2007;90(2):578–83.
- Bae S-G, Kim S, Jeong H, Lee Y, Jeong Y-G, Shin D-G. Effect of carbon and oxygen on the high-temperature properties of silicon carbide–hafnium carbide nanocomposite fiber. J Eur Ceram Soc. 2022;43(4):1385–96
- Sasikumar PVW, Blugan G, Casati N, Kakkava E, Panusa G, Psaltis D, et al. Polymer derived silicon oxycarbide ceramic

- monoliths: microstructure development and associated materials properties. Ceram Int. 2018;44(17):20961-7.
- 74. Rau AV, Knott K, Lu K. Porous SiOC/SiC ceramics via an activefiller-catalyzed polymer-derived method. Mater Chem Front. 2021;5(17):6530-45.
- 75. Wang K, Wang H, Cheng Y-B. Synthesis of nanostructured silicon carbide spheres from mesoporous C-SiO₂ nanocomposites. Chem Commun. 2009;46(2):303-5.
- 76. Poerschke DL, Braithwaite A, Park D, Lauten F. Crystallization behavior of polymer-derived Si-O-C for ceramic matrix composite processing, Acta Mater, 2018;147;329-41.
- 77. Leonel GJ, Guo X, Singh G, Navrotsky A. Compositional analysis of SiOC(H) powders: a comparison of X-ray photoelectron spectroscopy (XPS) and combustion analysis. Ceramics. 2023;6(1):74-85.
- 78. Michelle Morcos R, Mera G, Navrotsky A, Varga T, Riedel R, Poli F, et al. Enthalpy of formation of carbon-rich polymer-derived amorphous SiCN ceramics. J Am Ceram Soc. 2008;91(10):3349-54.
- 79. Mera G, Navrotsky A, Sen S, Kleebe H-J, Riedel R. Polymerderived SiCN and SiOC ceramics - structure and energetics at the nanoscale. J Mater Chem A. 2013;1(12):3826-36.
- 80. David L, Bhandavat R, Barrera U, Singh G. Silicon oxycarbide glass-graphene composite paper electrode for long-cycle lithium-ion batteries. Nat Commun. 2016;7(1):10998.
- 81. Zybill C, Handwerker H, Friedrich H. Silaorganometallic chemistry on the basis of multiple bonding. In: Stone FGA, West R, editors. Advances in organometallic chemistry. Vol. 36. Cambridge: Academic Press: 1994, p. 229-81.
- 82. Farnan I, Cho H, Weber WJ. Quantification of actinide α-radiation damage in minerals and ceramics. Nature. 2007;445(7124):190-3.
- 83. Widgeon S, Mera G, Gao Y, Sen S, Navrotsky A, Riedel R. Effect of precursor on speciation and nanostructure of SiBCN polymer-derived ceramics. J Am Ceram Soc. 2013;96(5):1651-9.
- 84. Berger F, Müller A, Aldinger F, Müller K. Solid-state NMR investigations on Si-B-C-N ceramics derived from boronmodified poly(allylmethylsilazane). Z Anorg Allg Chem. 2005;631(2-3):355-63.
- 85. Widgeon SJ, Sen S, Mera G, Ionescu E, Riedel R, Navrotsky A. ²⁹Si and ¹³C solid-state NMR spectroscopic study of nanometerscale structure and mass fractal characteristics of amorphous polymer derived silicon oxycarbide ceramics. Chem Mater. 2010;22(23):6221-8.
- 86. Widgeon S, Mera G, Gao Y, Stoyanov E, Sen S, Navrotsky A, et al. Nanostructure and energetics of carbon-rich SiCN ceramics derived from polysilylcarbodiimides: role of the nanodomain interfaces. Chem Mater. 2012;24(6):1181-91.
- 87. Xue J, Hu S, Li X, Li F, Liu Y, Wei H. Enhanced microwave absorbing properties of Y2O3 modified PDC SiCN ceramics with heterogeneous amorphous interface. J Alloys Compd. 2023;931:167499.
- 88. Jia Y, Chowdhury MAR, Xu C. Complex impedance spectra of polymer-derived SiC annealed at ultrahigh temperature. J Am Ceram Soc. 2020;103(12):6860-8.

- 89. Feng Y. Feng N. Wei Y. Bai Y. Preparation and improved electrochemical performance of SiCN-graphene composite derived from poly(silylcarbondiimide) as Li-ion battery anode. J Mater Chem A. 2014;2(12):4168-77.
- 90. Sang Z, Zhao Z, Su D, Miao P, Zhang F, Ji H, et al. SiOC nanolayer wrapped 3D interconnected graphene sponge as a high-performance anode for lithium ion batteries. J Mater Chem A. 2018;6(19):9064-73.
- 91. Chen J, King SW, Muthuswamy E, Koryttseva A, Wu D, Navrotsky A. Thermodynamic stability of low-k amorphous SiOCH dielectric films. J Am Ceram Soc. 2016:99(8):2752-9.
- 92. Morcos RM, Navrotsky A, Varga T, Ahn D, Saha A, Poli F, et al. Thermodynamically stable Si_wC_xN_yO_z polymer-like, amorphous ceramics made from organic precursors. J Am Ceram Soc. 2008;91(7):2391-3.
- 93. Tavakoli AH, Golczewski JA, Bill J, Navrotsky A. Effect of boron on the thermodynamic stability of amorphous polymer-derived Si(B)CN ceramics. Acta Mater. 2012;60(11):4514-22.
- 94. Varga T, Navrotsky A, Moats JL, Michelle Morcos R, Poli F, Müller K, et al. Thermodynamically stable Si_xO_vC_z polymerlike amorphous ceramics. J Am Ceram Soc. 2007;90(10):3213-9.
- 95. Morcos RM, Navrotsky A, Varga T, Blum Y, Ahn D, Poli F, et al. Energetics of Si_xO_vC_z polymer-derived ceramics prepared under varying conditions. J Am Ceram Soc. 2008;91(9):2969-74.
- 96. Tavakoli AH, Campostrini R, Gervais C, Babonneau F, Bill J, Sorarù GD, et al. Energetics and structure of polymer-derived Si-(B-)O-C glasses: effect of the boron content and pyrolysis temperature. J Am Ceram Soc. 2014;97(1):303-9.
- 97. Niu M, Wang H, Chen J, Su L, Wu D, Navrotsky A. Structure and energetics of SiOC and SiOC-modified carbon-bonded carbon fiber composites. J Am Ceram Soc. 2017;100(8):3693-702.
- 98. Ionescu E, Sen S, Mera G, Navrotsky A. Structure, energetics and bioactivity of silicon oxycarbide-based amorphous ceramics with highly connected networks. J Eur Ceram Soc. 2018;38(4):1311-9.
- 99. Tavakoli AH, Armentrout MM, Narisawa M, Sen S, Navrotsky A. White Si-O-C ceramic: structure and thermodynamic stability. J Am Ceram Soc. 2015;98(1):242-6.
- 100. Petry N-C, Ulrich AS, Feng B, Ionescu E, Galetz MC, Lepple M. Oxidation resistance of ZrB2-based monoliths using polymer-derived Si(Zr,B)CN as sintering aid. J Am Ceram Soc. 2022;105(8):5380-94.
- 101. Barrios E, Zhai L. A review of the evolution of the nanostructure of SiCN and SiOC polymer derived ceramics and the impact on mechanical properties. Mol Syst Des Eng. 2020;5(10):1606-41.

How to cite this article: Leonel GJ, Guo X, Singh G, Gervais C, Navrotsky A. Energetics and structure of SiC(N)(O) polymer-derived ceramics. J Am Ceram Soc. 2023;106:5086-5101.

https://doi.org/10.1111/jace.19153